

MSI: a visible multi-spectral imager for 1.6-m telescope of Hokkaido University

Makoto Watanabe^a, Yukihiko Takahashi^a, Mitsuteru Sato^a, Shigeto Watanabe^a,
Tetsuya Fukuhara^a, Ko Hamamoto^a, and Akihito Ozaki^a

^aDepartment of Cosmosciences, Hokkaido University,
Kita 10, Nishi 8, Kita-ku, Sapporo, Hokkaido 060-0810, Japan

ABSTRACT

We have built a visible multi-spectral imager (MSI) for the 1.6-m Pirka telescope of the Hokkaido University in Hokkaido, Japan. The instrument is equipped with two liquid crystal tunable filters and a 512×512 pixel EMCCD camera. One of the major purposes of this instrument is to obtain multi-spectral images (series of narrow-band images at many different wavelengths) of the solar planets rapidly. These tunable filters are a Lyot filter with liquid crystal variable retarders and thus can tune the transmitting wavelength rapidly without moving parts. Their spectral ranges are 400–720 nm and 650–1100 nm and the bandwidth is typically 10 nm on both filters. The EMCCD camera can obtain images at a frame rate of about 32 Hz, which also enables us to improve the spatial resolution with the shift-and-add or the Lucky imaging techniques. The field of view is 3.3×3.3 arcmin with a pixel scale of 0.39 arcsec pixel $^{-1}$. The instrument also has *UBVRI*-band broad-band filters and several narrow-band filters. MSI is mounted at the $f/12$ Cassegrain focus of the telescope. It had the first light on February 2011, and then have been used for several astronomical and planetary science programs as a major facility instrument at this telescope. We describe the design, construction, integration, and performance of this multi-spectral imager.

Keywords: imaging, tunable filter

1. INTRODUCTION

The Planetary and Space Group of the Department of Cosmosciences, the Graduate School of Science, at the Hokkaido University, constructed an 1.6-m diameter optical/infrared telescope named "Pirka" (Pirka means clean and beautiful in the Ainu language) in December 2010. This telescope is located at the Nayoro Observatory [Figure 1 (left)] of the Faculty of Science, the Hokkaido University, in 142.5° E longitude and latitude 44.4° N at 151 m above sea-level, situated at 220 km north-northeast from the Sapporo campus of the university. The building of the observatory have been built in cooperation with the Nayoro City, which is also equipped with several small amateur telescopes and planetarium for public use and is opened as a public observatory. The natural seeing size (FWHM in *R*-band) at the observatory is 1.3–2.3 arcsec (typically 1.8 arcsec in median). There is no rainy season in June, which is common in other islands of Japan, while there is a lot of snow in the winter season.

The Pirka telescope [Figure 1 (middle)] is intended to be used primary for the observations of the solar planets (for example, short-term and long-term monitoring of the atmosphere of the solar planets for meteorological studies). As an instrument in the visible region for these observations, we built the multi-spectral imager [MSI; Figure 1 (right)]. This instrument is designed to perform spatially resolved spectroscopy of extended objects such as solar planets, by obtaining multi-spectral images (series of narrow-band images at many different wavelengths) rapidly. MSI is always mounted at the Cassegrain focus of the Pirka telescope and is also a major facility instrument at this telescope. Therefore, it have been also used for several astronomical observations of astronomical objects, especially, time variable objects, such as supernovae, pulsars, X-ray binaries, and so on. The instrument had the first light on February 2011 soon after the first light of the Pirka telescope in December 2010. In this paper, we describe the design, construction, integration, and performance of this multi-spectral imager.

Further author information: (Send correspondence to M. W.)
M. W.: E-mail: mwata@ep.sci.hokudai.ac.jp



Figure 1. (Left) Nayoro Observatory of Hokkaido University, (middle) 1.6-m Pirka telescope, and (right) MSI mounted at Cassegrain focus of the telescope.

2. DESIGN OVERVIEW

MSI is installed at the folded Cassegrain focus ($f/12.0$) of the Pirka telescope. The layout of the optics after the Cassegrain fold mirror is shown in Figure 2, and the opto-mechanical layout is shown in Figure 3. Table 1 summarizes the major specifications of the instrument.

We adopted a refractive relay optics with a collimator and camera system, and we placed liquid crystal tunable filters (LCTFs; see Section 3) and conventional glass and interference filters in the collimated beam between the collimator and camera lens units. The focal length of the collimator is 162.7 mm, which was optimized to maximize the unvignetted field of view (FOV) of the instrument under the restriction on the aperture size (22.1 mm in diameter) of the LCTF unit. This collimator forms an image of the telescope pupil with a 13.5 mm diameter just after the LCTF unit. As camera lens units, we designed two units with different focal lengths; one is for the normal (low spatial resolution) mode and another is for the high resolution mode for the Lucky imaging.^{1,2} The camera lens unit of the normal mode has a focal length of 71.6 mm, and provides a FOV of 3.3×3.3 arcmin with a pixel scale of $0.389 \text{ arcsec pixel}^{-1}$. On the other hand, that of the hi-resolution mode has a focal length of 348.8 mm, and provides a FOV of 41×41 arcsec with a pixel scale of $0.080 \text{ arcsec pixel}^{-1}$ to sample the diffraction-limited PSF image at 1000 nm. The lenses of the collimator and camera units are designed and fabricated by Photocoding, Inc. The two camera units would be switchable, however, currently, only the normal mode's camera unit is fabricated.

For future upgrades, a grism and polarizer (such as a Wollaston prism) could be also installed into the collimated beam, and a slit or focal plane mask could be installed at the telescope focal plane for spectroscopic and polarimetric modes, however these modes are not yet implemented. For optical alignments and diagnostic purposes, the pupil imaging lens unit, which forms a telescope pupil image onto the CCD image plane, can be placed into the collimated beam.

The optical and opto-mechanical components are mounted in a box-shaped enclosure with dimensions of 500 (width) \times 450 (depth) \times 280 (height) mm (see Figure 3). MSI has currently one linear stage to select one of two LCTF units or to desert the unit, and two filter wheels for narrow-band filters (360, 365, 370, 380, and 390 nm, H α) and broad-band Johnson-Cousins *UBVRI* filters.³ The LCTF units and all filters are mounted on the inside of a thermal box, which keeps the temperature of the LCTF units and filters above about 15°C in order to maintain the LCTF units in their operating temperature against a lower ambient temperature (from below -30 to $+10^\circ\text{C}$) in the winter season at Nayoro and to reduce a change in center wavelengths of transmittance of the narrow-band interference filters. The camera unit is outside the enclosure and is mounted on the side plate of the enclosure box. On the opposite side, the control electronics (CCD power supply, motor controllers, and LCTF controllers) are mounted. The weight of the instrument is about 50 kg.

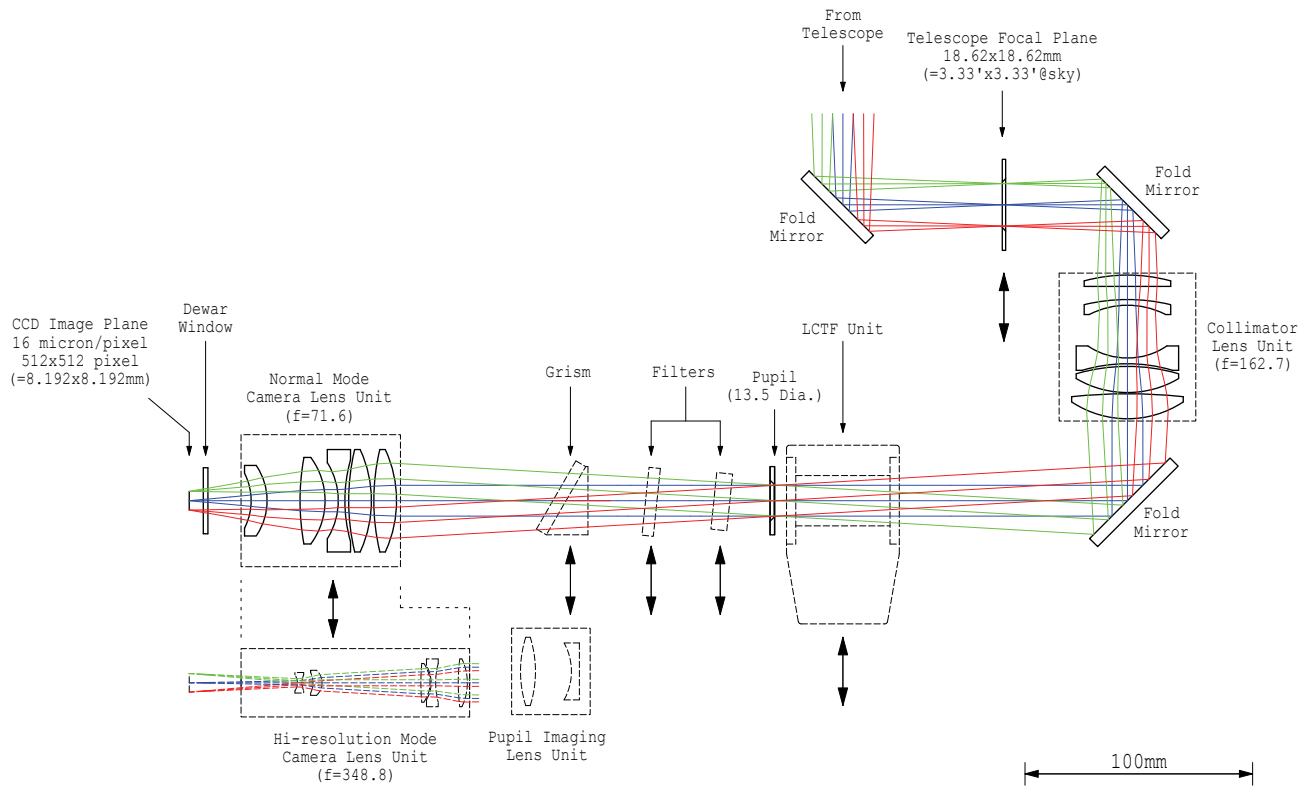


Figure 2. Optical layout of the multi-spectral imager.

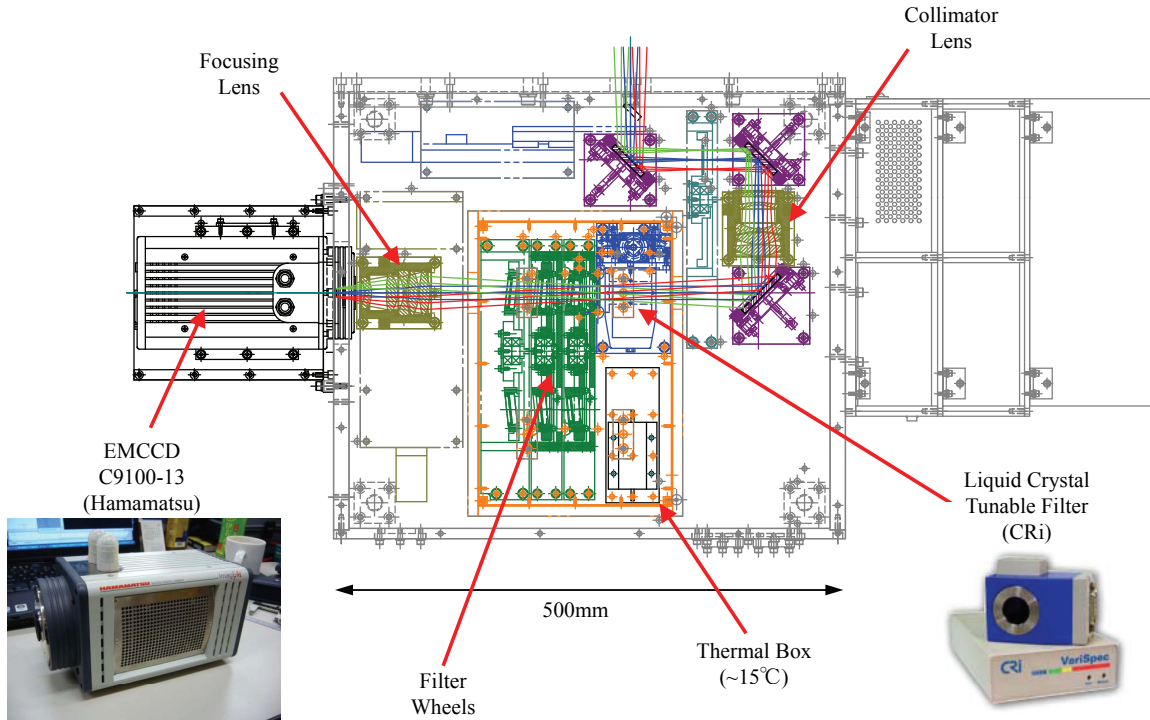


Figure 3. Opto-mechanical layout of the inside of enclosure of the instrument.

Table 1. Major specifications of multi-spectral imager.

Spectral coverage	360–1050 nm
Field of view	
Normal resolution mode	3.3×3.3 arcmin (0.389 arcsec pixel $^{-1}$)
High resolution mode	41×41 arcsec (0.080 arcsec pixel $^{-1}$)
Filters	
Liquid crystal tunable filters	CRi VariSpec VIS-10: 400–720 nm, $\Delta\lambda \sim 10$ nm (@ 650 nm), CRi VariSpec SNIR-10: 650–1100 nm, $\Delta\lambda \sim 10$ nm (@ 900 nm)
Narrow-band filters	360, 365, 370, 380, 390 nm ($\Delta\lambda = 10$ nm), H α ($\Delta\lambda = 1$ nm)
Broad-band filters	Johnson-Cousins <i>U, B, V, R, I</i>
Camera (CCD)	Hamamatsu Photonics C9100-13 (e2v CCD97 back-illuminated Electron Multiplying CCD)
Array format	512×512 pixel (Pixel size: $16 \times 16 \mu\text{m}$)
Readout modes	EMCCD mode, Normal CCD mode
Pixel clock rates	11 MHz (EMCCD mode only), 0.69 MHz, 2.75 MHz
Maximum frame rates (full-frame)	31.9 frames s $^{-1}$ (EMCCD mode), 2 frames s $^{-1}$ (Normal CCD mode)
Minimum exposure times (full-frame)	0.031 s (EMCCD mode), 0.488 s (Normal CCD mode)
EM gain	4–1200
CCD cooling method & temperature	Peltier with forced-air, -65°C
Outer dimensions	500 (W) \times 450 (D) \times 280 (H) mm (only enclosure) 995 (W) \times 464 (D) \times 333 (H) mm (including camera and electronics)
Weight	50 kg

3. LIQUID CRYSTAL TUNABLE FILTERS (LCTFS)

The LCTF units of MSI are commercial products (VariSpec* VIS-10-HC-20 and SNIR-10-HC-20) from Cambridge Research & Instrumentation, Inc. (CRi, currently part of Caliper Life Sciences, Inc.). These tunable filters are a series of Lyot filters with a liquid crystal retarder (and a fixed retarder) sandwiched by linear polarizers. The amounts of retardances of the liquid crystal retarders can be controlled electrically, and thus the LCTF can tune the transmitting wavelength rapidly without moving parts. The time taken to switch from one wavelength to another (response time) is typically only 50 and 150 ms for the VIS and SNIR units, respectively, at room temperature. The spectral ranges of our LCTF units are 400–720 nm (for the VIS unit) and 650–1100 nm (for the SNIR unit) and the bandwidth is typically 10 nm for both units. The center wavelength can be given by a value with a resolution of 0.001 nm within these spectral ranges through the USB interface, and the tuning accuracy of wavelength is the actual bandwidth/ 8 ± 0.5 nm, that is, typically 1.8 nm.

Figure 4 shows the curves of transmittance of linearly polarized light for our LCTFs with various settings of center wavelength, which are provided by manufacturer (note the transmittance of unpolarized light is an half of that of polarized light). The peak values of transmittance are roughly 50% for the VIS unit at 600–720 nm and for the SNIR unit at 700–1100 nm, but they become smaller at shorter wavelengths, especially for the VIS unit. Each transmittance curve is close to a Gaussian profile. The out-of-band transmittance is below 0.1%, but there are a secondary peak of transmittance at 710–750 nm for the SNIR unit when the setting of center wavelength is longer than 990 nm.

The bandwidth varies within a range of ~ 5 –19 nm and ~ 5 –15 nm for the VIS and SNIR units, respectively, depending on the setting of center wavelength. Figure 5 shows the FWHM of pass-band of our LCTFs, which is derived by approximating the transmittance curve to a Gaussian profile. The bandwidth varies linearly with setting of center wavelength, and gets narrower as a shorter center wavelength is selected. The relationship between FWHM (in nm) and center wavelength (λ_c in nm) can be described approximately as follows.

$$\text{FWHM} = \begin{cases} 3.9 + 0.042(\lambda_c - 400) & (\text{for VIS unit}) \\ 4.2 + 0.023(\lambda_c - 650) & (\text{for SNIR unit}) \end{cases}$$

The equivalent width of the pass-band is given by $(\sqrt{\pi/\ln 2})/2$ FWHM = 1.064 FWHM.

*<http://www.caliperls.com/products/microscopy-imaging-analysis/optical-components/varispec.htm>

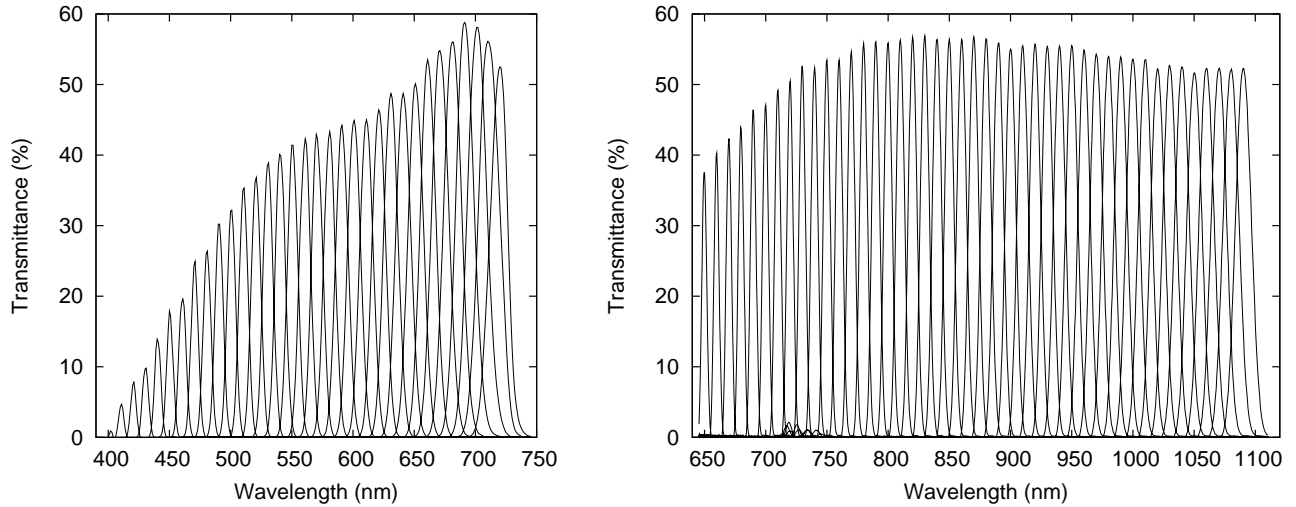


Figure 4. Transmittance curves of linearly polarized light for VIS (left) and SNIR (right) units of MSI's LCTFs with various settings of center wavelength.

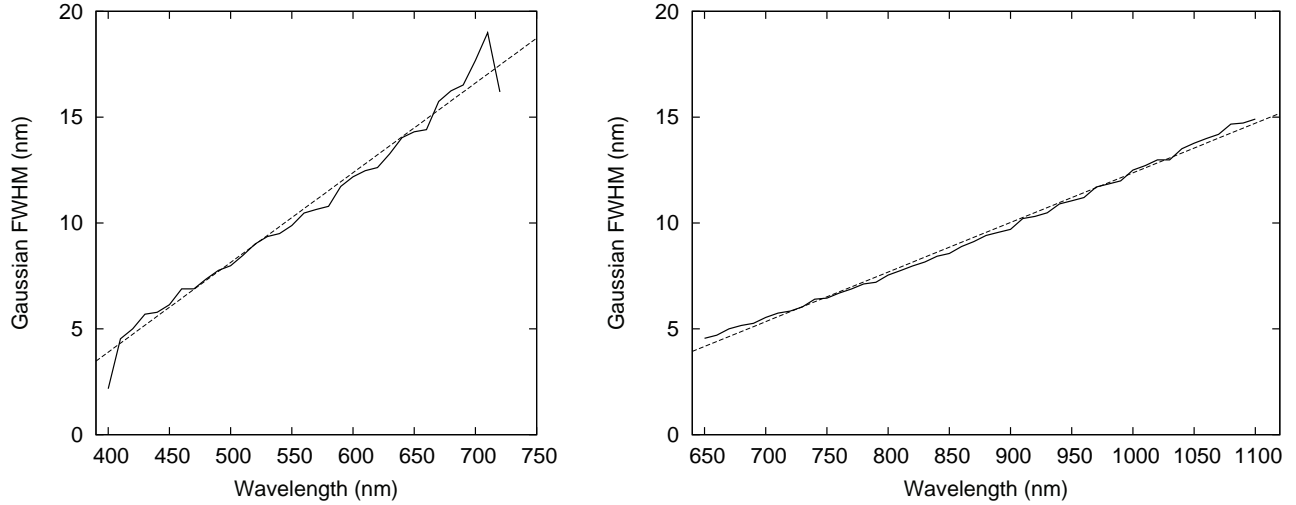


Figure 5. FWHM (solid curve) of pass-band of VIS (left) and SNIR (right) units of MSI's LCTFs with various setting of center wavelength, which is derived by approximating the transmittance curve to a Gaussian profile. The dashed line presents a linear fitting to solid curve.

4. EMCCD CAMERA

As the camera unit of the instrument, we adapted a commercial electron multiplying CCD (EMCCD) camera, C9100-13[†] (Hamamatsu Photonics K.K.). This camera has a back-illuminated frame-transfer CCD of e2v technologies, CCD97, which has 512×512 image pixels with a pixel size of $16 \times 16 \mu\text{m}$. The CCD is cooled by Peltier cooler with forced-air cooling, and the temperature is stabilized at -65°C within $\pm 0.03^\circ\text{C}$, and then the dark current is fairly small (about $0.01 \text{ e}^- \text{ s}^{-1}$). The camera is connected to an Windows PC via a CameraLink interface, and is controlled by the HiPic image acquisition software of Hamamatsu Photonics. This software can accept control commands remotely from the main control software of MSI through a TCP port.

The camera has two readout modes; a high frame rate EMCCD readout through multiplication registers and

[†]http://jp.hamamatsu.com/products/camera/pd343/5011/imagemb/index_en.html

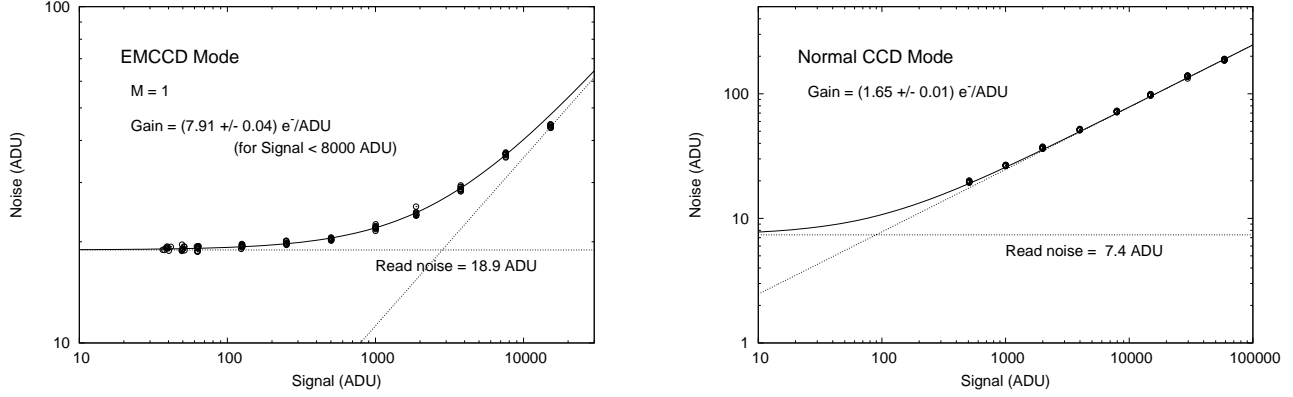


Figure 6. Measured photon transfer curve for EMCCD mode with $M = 1$ (left) and normal CCD mode (right).

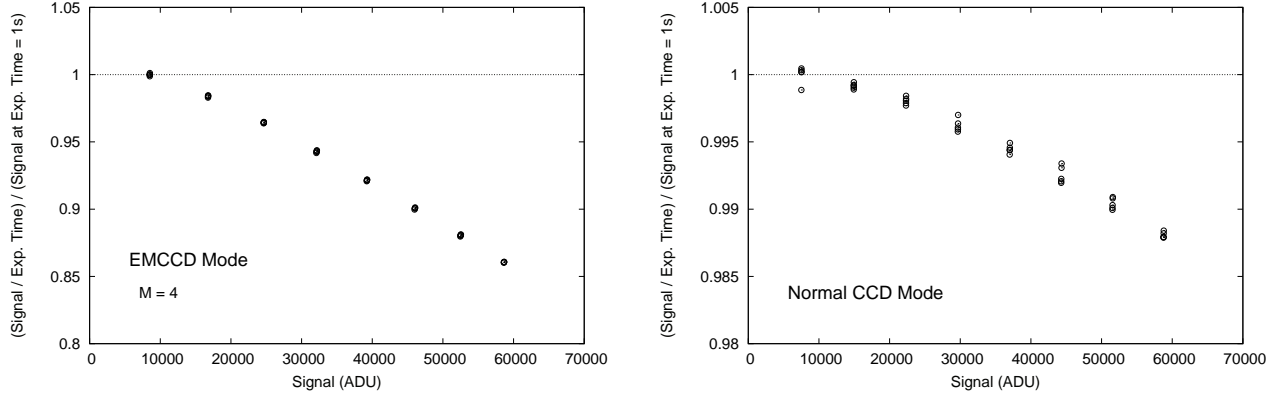


Figure 7. Measured linearity for EMCCD mode with $M = 4$ (left) and normal CCD mode (right).

a low-noise normal CCD readout without multiplication for the conventional CCD operation. Three setting of a pixel clock rate of 11 (only for EMCCD readout), 2.75, and 0.69 MHz are selectable, enabling us to obtain full-frame images at a frame rate of 31.9, 8.0, and 2.0 frames s $^{-1}$, respectively, at maximum. These set also the minimum exposure time of 0.031, 0.122, and 0.488 s, respectively, for the full-frame readout. By using pixel binning and/or partial (sub-array) readout, a higher frame rate or shorter exposure time can be used.

Table 2 shows the measured readout noise of the EMCCD camera of MSI. For the EMCCD readout, the measurements were done with the minimum EM gain ($M = 4$), and the measured values were reduced into equivalent values at input by dividing with the M value.

Table 2. Measured readout noise.

Readout Mode	EM Gain	Pixel Clock Rate (MHz)	Readout Noise (e $^-$)	
			Measured	Catalog
EMCCD	4	11	33	25
EMCCD	4	2.75	27	20
EMCCD	4	0.69	12	8
Normal CCD		2.75	21	17
Normal CCD		0.69	13	8

We derived the CCD gain (AD conversion factor) of our camera from the photon transfer curve shown in Figure 6. For the EMCCD mode, the measurement was done with the calibration mode of the HiPic software to

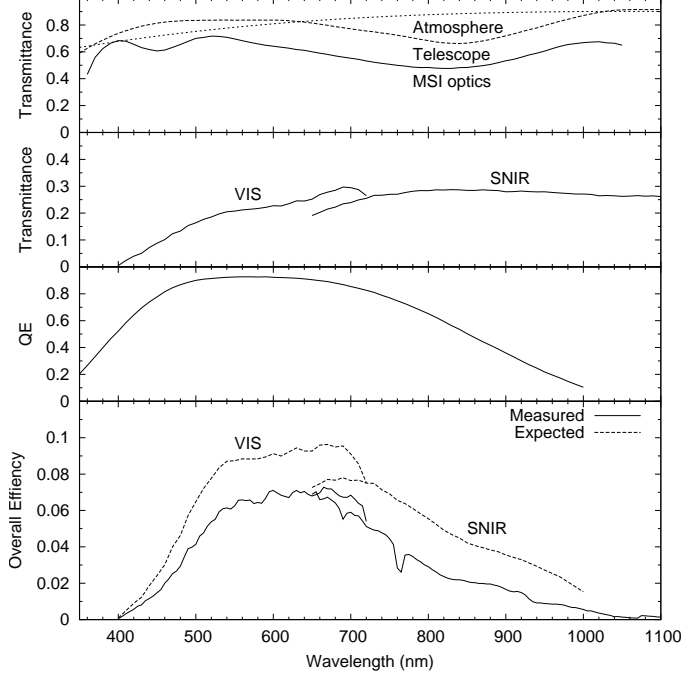


Figure 8. Expected transmittance of atmosphere, telescope, and MSI optics (top), transmittance of filters (upper middle), CCD quantum efficiency (lower middle) and overall efficiency (bottom).

set $M = 1$. We confirmed that the derived values of 7.91 (for the EMCCD mode) and $1.65 \text{ e}^- \text{ ADU}^{-1}$ (for the normal CCD mode) are close to the catalog values (5.8 and $1.4 \text{ e}^- \text{ ADU}^{-1}$ for the EMCCD and normal CCD modes, respectively). We checked also the linearity of CCD. Figure 7 shows the linearity curve derived from flat-field lamp images with various exposure times. For the EMCCD mode, a large non-linearity (about 15% at 60000 ADU) is shown because the effective EM gain is decreased by charge of photo-electrons in an EM register. For the normal mode, the non-linearity is small and < 1% below 50000 ADU.

5. PERFORMANCES AND EXAMPLES OF OBSERVATIONS

5.1 Multi-spectral Imaging

Figure 8 shows the optical efficiency of the instrument. The overall efficiency was measured by multi-spectral imaging of an A0V-type star. It is 0.04–0.06 in the range of 500–750 nm and becomes below an half of it at the other wavelengths. The measured overall efficiency was lower than the expected one. It might be due to the poor photometric condition at this observation and the further investigation is needed.

Figure 9 shows the estimates of limiting magnitude at S/N (signal-to-noise ratio) = 10 for the multi-spectral imaging with the LCTFs. The estimates for an extended objects and point source with both of the EMCCD[‡] and normal CCD modes, several exposure times, and EM gains are presented. For example, Jupiter and Saturn have a surface brightness of roughly 5.3 and 6.5 mag arcsec⁻², respectively, at the V -band. MSI has a sufficient performance even with a very short exposure time such as 0.031 s for these objects in the most of the wavelength range by virtue of EMCCD.

[‡]For the EMCCD mode, the S/N ratio is calculated by $S/N = N_* t / \sqrt{F^2[N_* + n_{\text{pix}}(N_s + N_d)]t + n_{\text{pix}}(\sigma_r/M)^2}$, where N_* is the total number of photo-electrons per second collected from the object, N_s is the number of sky or background photo-electrons per pixel per second, N_d is the number of dark current electrons per pixel per second, σ_r is the readout noise at output in electrons, n_{pix} is the number of pixels under consideration for the S/N calculation, t is the exposure time in seconds, F is the excess noise factor ($F = \sqrt{2}$), and M is the EM gain.

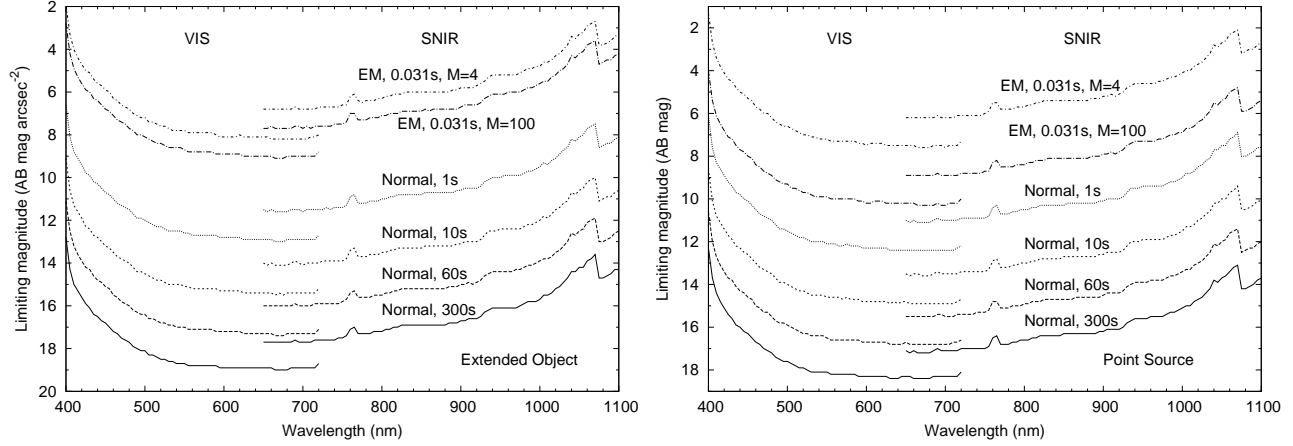


Figure 9. Estimates of limiting magnitude at $S/N = 10$ for multi-spectral imaging with LCTFs. Estimates for an extended object (left) and point source (right) with 0.031 s exposure with EMCCD mode ($M = 4$ and $M = 100$), and 1, 10, 60, and 300 s exposure with normal CCD mode are shown (from upper to lower curves). For a point source, 4 arcsec diameter aperture and 2 arcsec seeing are assumed.

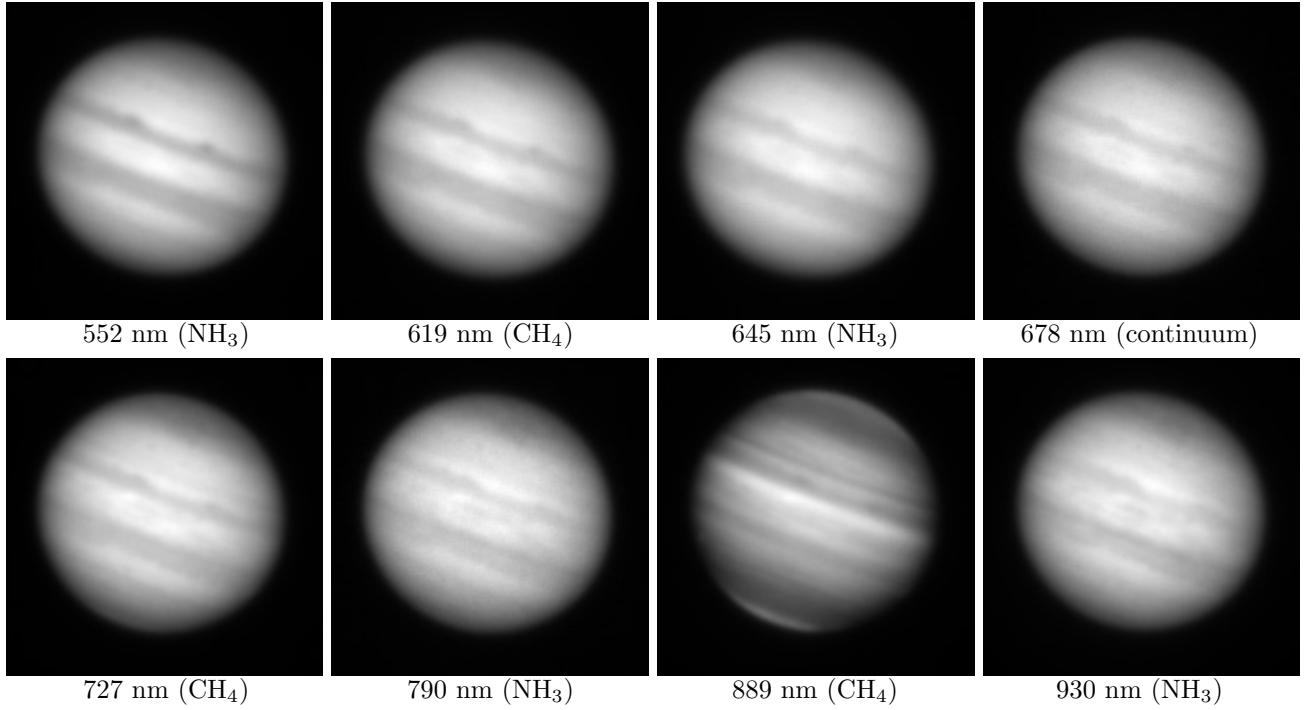


Figure 10. Jupiter's images at several CH_4 and NH_3 absorption bands obtained by multi-spectral imaging with MSI.

Figure 10 shows an example of multi-spectral imaging of Jupiter, which are taken at several methane and ammonia absorption bands and continuum. Difference of spatial features between the wavelengths are clearly shown. Another example of multi-spectral imaging of Saturn is shown in Figure 11, demonstrating the performance of the spatially resolved spectroscopy of an extended object. The several methane absorption bands are clearly shown. The scan of wavelength is done from 400 to 720 nm and from 650 to 1100 nm with an interval

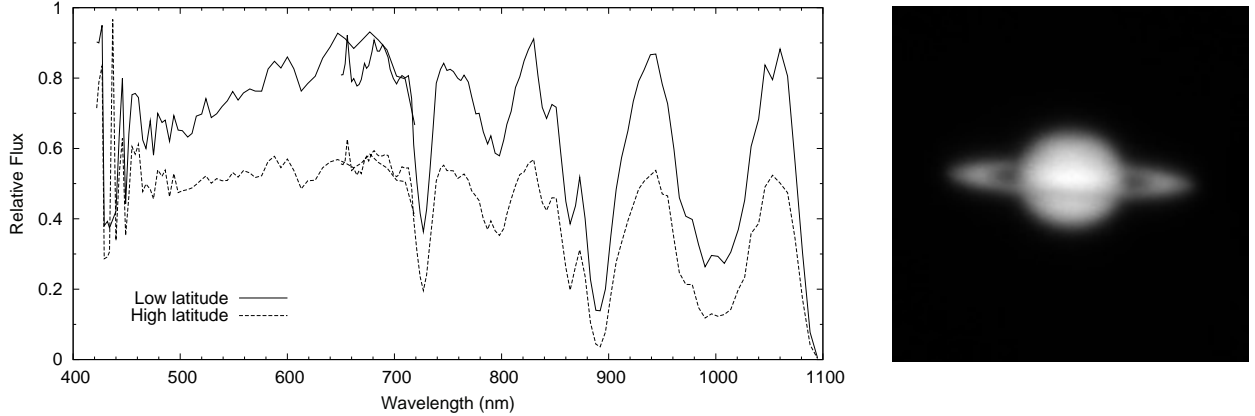


Figure 11. Saturn's spectra (left) at two different latitudes and image at 677 nm (right) obtained by multi-spectral imaging with MSI.

of 2–9 and 2–7 nm, resulting narrow-band images at 71 and 109 different wavelengths with the VIS and SNIR units, respectively. The exposure time of each image was 0.1 s and three cycles of the scan were done. The time taken to obtain a set of images was about 208 s with the VIS unit and 328 s with the SNIR unit each cycle, and thus about 3 s is taken per image. Currently, most of the time is spent for creating image files, and we are planning to increase the speed of scanning by improving the control software.

5.2 Lucky Imaging

In Nayoro, the Fried coherent length r_0 has only 16 cm even at the good seeing condition (1.3 arcsec) and the longest wavelength of this instrument (1000 nm), and thus $D = 10r_0$ (where D is the aperture diameter of telescope). For this situation, the probability of obtaining a good short-exposure image is only one in 10^6 (see Ref. 1), therefore, we are not expecting a diffraction-limited performance in our Lucky imaging mode, but we are expecting some improvement of the angular resolution with a factor of 2–4 by Lucky imaging and shift-and-add technique, as described in Ref. 4 for their poor seeing condition. At this moment, our Lucky imaging mode is not well evaluated, and therefore the further investigation is needed.

5.3 Broad-band Imaging

As mentioned in Section 1, MSI is also used for broad-band imaging, frequently. Table 3 summarizes the measured overall efficiency (including the transmittance of atmosphere at airmass = 1) and estimates of limiting magnitude at $S/N = 10$ with various exposure times t and EM gains M for an extended object and a point source.

We also derived the color equations transforming from the instrumental magnitudes to the Landolt system.⁷ The following is a tentative result derived from observations in only one night:

$$\begin{aligned}
 u &= U + (4.032 \pm 0.044) + (0.467 \pm 0.028)X + (-0.286 \pm 0.009)(U - B), \\
 b &= B + (1.060 \pm 0.022) + (0.378 \pm 0.015)X + (-0.111 \pm 0.004)(B - V), \\
 v &= V + (0.771 \pm 0.021) + (0.277 \pm 0.015)X + (0.097 \pm 0.007)(V - R), \\
 r &= R + (1.021 \pm 0.024) + (0.197 \pm 0.017)X + (0.146 \pm 0.010)(R - I), \\
 i &= I + (2.022 \pm 0.028) + (0.146 \pm 0.019)X + (-0.046 \pm 0.013)(R - I),
 \end{aligned}$$

where u, b, v, r , and i are the instrumental magnitudes defined by $25 - 2.5 \log_{10} I$ (where I is the received counts in ADU s^{-1}), U, B, V, R, I , and $U - B, B - V, V - R, R - I$ are the magnitudes and colors in the Landolt system, and X is the airmass.

Table 3. Limiting magnitude ($S/N = 10$) for broad-band imaging.

	<i>U</i>	<i>B</i>	<i>V</i>	<i>R_C</i>	<i>I_C</i>
Effective wavelength ^a (nm)	366	438	545	641	798
Effective bandwidth ^b (nm)	61	94	87	149	146
Sky brightness (mag arcsec ⁻²)	21.5	21.5	20.4	20.1	18.8
Overall efficiency	0.030	0.176	0.381	0.270	0.179
Limiting magnitude for extended source (Vega mag arcsec ⁻²)					
EMCCD mode ($t = 0.031$ s, $M = 4$)	8.6	11.7	12.1	11.9	10.9
EMCCD mode ($t = 0.031$ s, $M = 100$)	9.5	12.5	12.9	12.7	11.8
Normal CCD mode ($t = 1$ s)	13.4	16.4	16.8	16.6	15.7
Normal CCD mode ($t = 10$ s)	15.9	18.9	19.1	19.0	18.0
Normal CCD mode ($t = 60$ s)	17.8	20.6	20.7	20.5	19.4
Normal CCD mode ($t = 300$ s)	19.4	21.9	21.7	21.6	20.5
Limiting magnitude for point source ^c (Vega mag)					
EMCCD mode ($t = 0.031$ s, $M = 4$)	8.0	11.0	11.4	11.3	10.3
EMCCD mode ($t = 0.031$ s, $M = 100$)	10.7	13.7	14.1	13.9	13.0
Normal CCD mode ($t = 1$ s)	12.8	15.9	16.3	16.1	15.1
Normal CCD mode ($t = 10$ s)	15.3	18.3	18.6	18.4	17.4
Normal CCD mode ($t = 60$ s)	17.3	20.0	19.9	19.8	18.7
Normal CCD mode ($t = 300$ s)	18.9	21.2	20.9	20.7	19.6

^a From Ref. 5.

^b From Ref. 6.

^c 4 arcsec diameter aperture and 2 arcsec seeing are assumed.

6. CONCLUSIONS

We have built a multi-spectral imager for the 1.6-m Pirka telescope. It consists of the combination of the LCTFs and EMCCD camera. This simple and unique combination allows us to perform spatially resolved spectroscopy of extended objects easily without involving of construction of a complicated integral field unit such as an image slicer. While the spectral resolution of the multi-spectral imaging with this instrument is rather low, the spectral coverage is wide enough to cover almost all the visible region. Thus, this instrument is suited for obtaining spatially-resolved spectral energy distribution of extended objects over the whole of the visible region.

ACKNOWLEDGMENTS

The Pirka telescope is operated by Graduate School of Science, Hokkaido University. It also participates in the Optical & Near-Infrared Astronomy Inter-University Cooperation Program, supported by the MEXT of Japan.

REFERENCES

- [1] Fried, D. L., “Probability of getting a lucky short-exposure image through turbulence,” *JOSA* **68**, 1651–1657 (1978).
- [2] Baldwin, J. E., Tubbs, R. N., Cox, G. C., Mackay, C. D., Wilson, R. W., & Andersen, M. I., “Diffraction-limited 800 nm imaging with the 2.56 m Nordic Optical Telescope,” *A&A* **368**, L1–L4 (2001).
- [3] Bessell, M. S., “UBVRI passbands,” *PASP* **102**, 1181–1199 (1990).
- [4] Law, N. M., Mackay, C. D., & Baldwin, J. E., “Lucky imaging: high angular resolution imaging in the visible from the ground,” *A&A* **446**, 739–745 (2006).
- [5] Bessell, M. S., Castelli, F., & Plez, B., “Model atmospheres broad-band colors, bolometric corrections and temperature calibrations for O-M stars,” *A&A* **333**, 231–250 (1998).
- [6] Fiorucci, M., & Munari U., “The Asiago database on photometric systems (ADPS) II. band and reddening parameters,” *A&A* **401**, 781–796 (2003).
- [7] Landolt, A. U., “UBVRI photometric standard stars around the celestial equator: updates and additions,” *AJ* **137**, 4186–4269 (2009).